The snow and rainfall impact on the Verde spring behavior: a statistical approach on hydrodynamic and hydrochemical daily time-series

Alessandro Chiaudani[1], Diego Di Curzio[1] and Sergio Rusi[1*]

[1]Department of Engineering and Geology (InGeo), University “G. d’Annunzio” of Chieti-Pescara, Via dei Vestini, 30 - 66013 Chieti, Italy;

Emails: alessandro.chiaudani@unich.it; diego.dicurzio@unich.it

*Corresponding author: sergio.rusi@unich.it

*Graphical Abstract

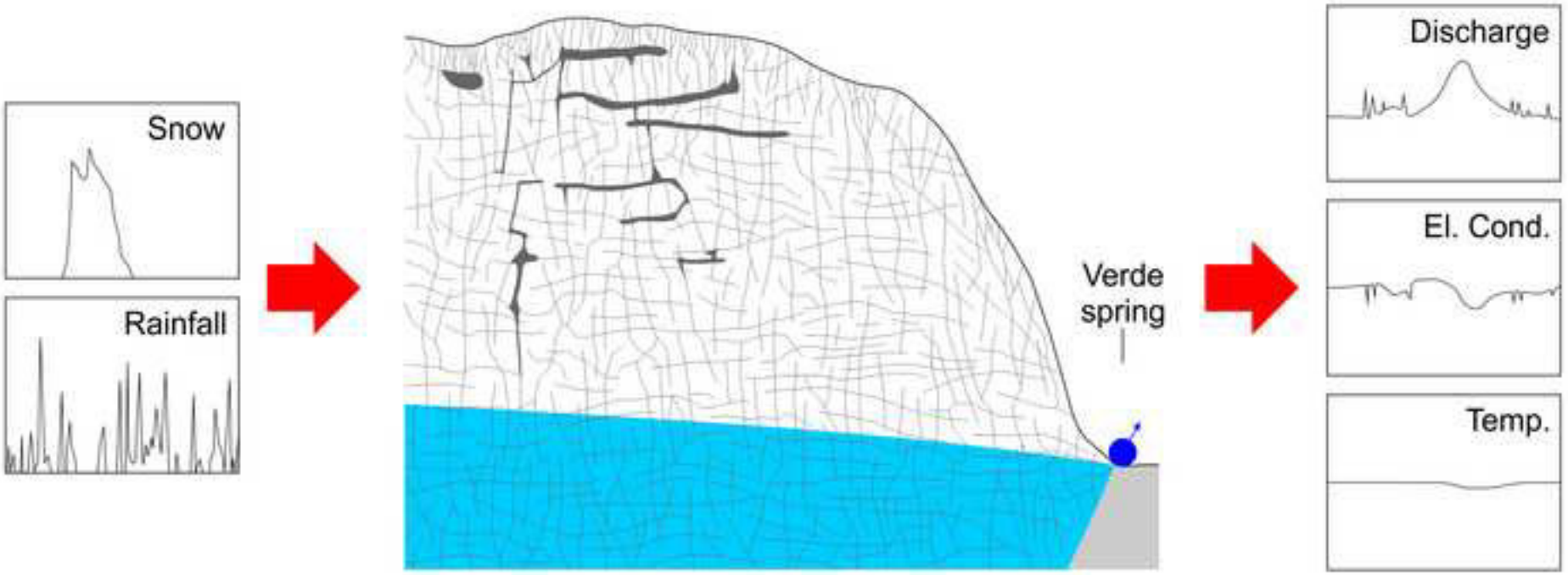

***Highlights (for review : 3 to 5 bullet points (maximum 85 characters including spaces per bullet point)**

Highlights

- It was highlighted the major role of the snowmelt on the aquifer recharge
- The recharge causes changes in the hydrodynamic and hydrochemical spring parameters
- The statistical analysis identified recharge modes related to different flow paths
- The flow paths are characterized by different sizes and hydrodynamic properties

The snow and rainfall impact on the Verde spring behavior: a statistical approach on hydrodynamic and hydrochemical daily time-series

Alessandro Chiaudani[1], Diego Di Curzio[1] and Sergio Rusi[1*]

[1]Department of Engineering and Geology (InGeo), University "G. d'Annunzio" of Chieti-Pescara, Via dei Vestini, 30 - 66013 Chieti, Italy;

Emails: alessandro.chiaudani@unich.it; diego.dicurzio@unich.it

*Corresponding author: sergio.rusi@unich.it

Abstract

The regional wide aquifer system springs are one of the most important sources of freshwater, especially because of the ever-increasing global water demand. Thus, these springs must be protected and managed in a sustainable manner. To this purpose, a detailed knowledge about the corresponding aquifer systems hydrodynamic is vital.

In this general framework, the main objective of this research is to get a deeper insight into the hydrogeological conceptual model of the Verde spring, that is the most important spring of the Majella carbonate aquifer in Central Italy. This aquifer system is characterized by a heterogeneous hydraulic conductivity distribution and groundwater flow, and its recharge is mainly due to both rainfall and snowmelt.

The raw and residual multiparameter time-series, related to the input (i.e. rainfall, snow cover thickness) and output (i.e. spring discharge, groundwater temperature and electrical conductivity) parameters of this aquifer, were analyzed by means of statistical techniques, such as autocorrelation and cross-correlation.

The results obtained by this methodological approach highlighted that the snowmelt is the most important inflow of the Majella aquifer system. The snow cover melting leaks slowly large amount of water into the aquifer and creates smoothly significative modifications to

the spring discharge, electrical conductivity and temperature, in terms of groundwater volume increase and dilution. Contrariwise, although the rainfall inflow volume and the corresponding spring parameters changes are very limited, the transient behavior of the rainfall inflow allowed to identify different recharge modes. These recharge modes depend on several flow paths in the unsaturated zone, characterized by different water volumes brought toward the saturated zone, sizes, hydraulic conductivities, and distances from the Verde spring.

Keywords: groundwater; hydrogeological conceptual model; aquifer recharge; spring behavior; multiparameter dataset; time-series analysis

Introduction

In the last decades, the global economic development has rapidly increased population growth, industrialization and urbanization, generating an ever-increasing demand for freshwater resources (MEA, 2005; WWAP, 2015). In this framework, the regional aquifer system springs are one of the most important sources of freshwater, due to aquifer large volumes and high storage capacities. Since they are highly sensitive to meteo-climatic changes (Dragoni and Sukhija, 2008), getting a deeper insight into the aquifer hydrodynamic allows to protect freshwater resources and manage their exploitation in a sustainable manner.

Due to the great heterogeneity of carbonate aquifers, their groundwater flow paths are often described in detail by artificial or environmental tracer tests (Kresic and Stevanovic, 2009), where logistic conditions and environmental restrictions allow their implementation. However, even spring discharge patterns reflect the physical processes and the aquifer properties that influence groundwater flow. For this purpose, the analysis of their

hydrographs is a common and effective way for evaluating the features of different aquifers feeding these springs (Brutsaert and Nieber, 1977; Mangin, 1984; Pinault et al., 2001; Fiorillo, 2009, 2011; Galleani et al., 2011; Jukìc and Denić-Jukić, 2015; Posavec et al., 2017).

Scientific research on time-series is usually focused on hydrogeological processes concerning relations between input (e.g. precipitation) and output (e.g. spring discharge or hydraulic heads) in fractured and/or karstic (Box et al., 1994; Padilla and Pulido-Bosch, 1995; Larocque et al., 1998; Panagopoulos and Lambrakis, 2006; Delbart et al., 2013) and porous aquifer systems (Lo Russo et al., 2014; Chiaudani et al., 2017). The study of these relations provides useful information to get a deeper insight into aquifer system features, such as recharge modes, flow paths in the aquifer, flow regime, hydraulic conductivity and/or thickness of the unsaturated zone, recharge area extent, that allow to implement a more detailed conceptual model of groundwater flow (Obarti et al., 1988; Larocque et al. 2000, 2001; Aquilina et al. 2006; Liu et al., 2010; Daher et al., 2011; Basagaoglu et al., 2015). From a methodological point of view, these relations are generally investigated by means of univariate and bivariate time-series analyses. Among others, the Cross-Correlation Function provides the response time of output time-series to input variations (Mangin, 1984; Laroque et al., 1998; Panagopoulos and Lambrakis, 2006; Duvert et al., 2015). In addition, this analysis points out the effective weight of input variation on the output behavior (e.g. rainfall recharge on hydraulic heads fluctuation as in Chiaudani et al 2017).

Most of the literature considers rainfall as the main input of aquifer systems or deep and lateral inflow (Thanh Tam et al., 2004; Di Curzio et al, 2016; Viaroli et al, 2018), although in many cases, especially in wide regional aquifers characterized by high elevations, snowfall supply the major water volume during the recharge (Nanni and Rusi, 2003; Petitta et al, 2018; Rusi et al, 2018). In fact, the snow cover, melting after a long period of

77 accumulation on the recharge area ground, plays a significant role in the storage and
78 redistribution of water resources within regional groundwater flow systems, (Bayard et al.,
79 2005; Fiorillo et al, 2015; Meeks and Hunkeler, 2015).
80 In addition to the volumetric variation, the recharge causes changes in physico-chemical
81 properties of spring water, such as temperature (T) and electrical conductivity (EC),
82 because of the differences in these parameters of both rainfall and snowmelt that infiltrate
83 in the aquifer. Since the more infiltrating volumes are large, the more physico-chemical
84 properties of groundwater will change, the time responses of hydraulic head and/or spring
85 discharge fluctuation should be compared with the ones of physico-chemical parameters,
86 in order to improve the conceptual model by new detailed information.
87 For this reason, the main objective of this study is to detail the previous hydrogeological
88 conceptual model of the Verde spring, that is the most important spring of the Majella
89 carbonate aquifer system in Central Italy (Nanni and Rusi, 2003), comparing univariate
90 and bivariate statistical analyses of multiparameter (i.e. rainfall, snow cover thickness,
91 spring discharge, groundwater temperature and electrical conductivity) time-series.
92

93 **Material and methods**

94 *Study area*

95 The Majella massif (Nanni and Rusi, 2003; Fiorillo et al. 2015; Liberatoscioli et al, 2018) is
96 located in central Apennines (Italy) and is one of the larger carbonate aquifers in Central
97 Italy, with an extension of 273 km^2 (Fig. 1).
98 From a geological point of view, this massif is made up by a wide sequence (thickness ~2
99 km) of carbonate formations (Jurassic-Miocene), whose lithological properties vary
100 depending on deposition paleo-environments (Crescenti et al. 1969). In fact, the older
101 strata (up to Paleogene) are mainly platform and slope-to-basin limestones, while the more
102 recent ones are ramp limestones and marls (Volatili et al., 2019 and relative bibliography).

During the Apennines uplift in middle-to-late Miocene, the Mediterranean geodynamic evolution strongly deformed the carbonate rocks, creating the Majella arc-shaped asymmetric anticline. Throughout the orogenic phase, the Majella anticline overlapped, by an east-verging thrust system, younger marine terrigenous formations (Miocene), that are mainly constituted by clayey-arenaceous and evaporitic deposits (Ghisetti and Vezzani, 1997). During the Quaternary age, this anticline was progressively cut, especially in the western part, by a normal-fault system that juxtaposed the carbonate rocks with the terrigenous deposits (Calamita et al., 2002; Scisciani et al., 2002). In addition, the tectonic deformation created internal discontinuities and heterogeneities, such as several sets of differently open fractures, pressure solution seams and deformation bands (Volatili et al., 2019), which favored the development of karst. Furthermore, on the upper plains and along the slopes of the massif, variably thick head sediments were deposited (Scisciani et al., 2000).

The complex geological features developed during the orogenesis influence the hydraulic properties and the groundwater flow of the Majella aquifer. As a matter of fact, this aquifer system is laterally isolated by the regional tectonic systems (i.e. thrusts and normal faults). Nevertheless, since in the northern part the geological structures are still quite unclear, hydraulic continuity cannot be excluded (Nanni and Rusi, 2003). In addition, the limestone, variably weathered by fractures and karst, are the more permeable complex (secondary porosity) and represent the actual aquifer. Within these rocks, the groundwater flow is very heterogeneous, because of the combination of several flow paths, each one characterized by different hydraulic conductivity and continuity. Both in the unsaturated and the saturated zones, variably large and continuous conduits or fractures and heterogeneous fracture networks coexist and contribute different water volumes and flow velocities to the overall groundwater circulation. This is demonstrated by the presence of more than 240 springs.

128 The Majella aquifer has a total spring discharge of about 8 m^3/s, while the net recharge is
129 more than 900 mm/year, with respect to an average rainfall of about 1450 mm/year. The
130 net recharge of this aquifer is exclusively due to snowfall and rainfall, without any water
131 yield from other adjacent carbonate aquifers (Nanni and Rusi, 2003). Most of the Majella
132 aquifer water volumes leaks out through few basal springs (Fig. 1), that are located in the
133 eastern and northern sides of the massif, with average discharges varying from 0.6 to 3.5
134 m^3/s. All the investigations (Celico, 1978; Nanni and Rusi, 2003) indicate that these are
135 recharged by flow paths of a single heterogeneous aquifer, whose dimensions, volumetric
136 capacity, and depth increase northward.
137 Among others, the Verde spring (VS) is the most important one, in terms of discharge,
138 likely because it has the lowest elevation with respect to the other basal springs. Its
139 groundwater is exploited for drinking purposes (about 25%) and for hydroelectric power
140 production. This spring is located in the central part of the tectonic interface between the
141 carbonate aquifer and the terrigenous aquiclude, under the head deposits.
142

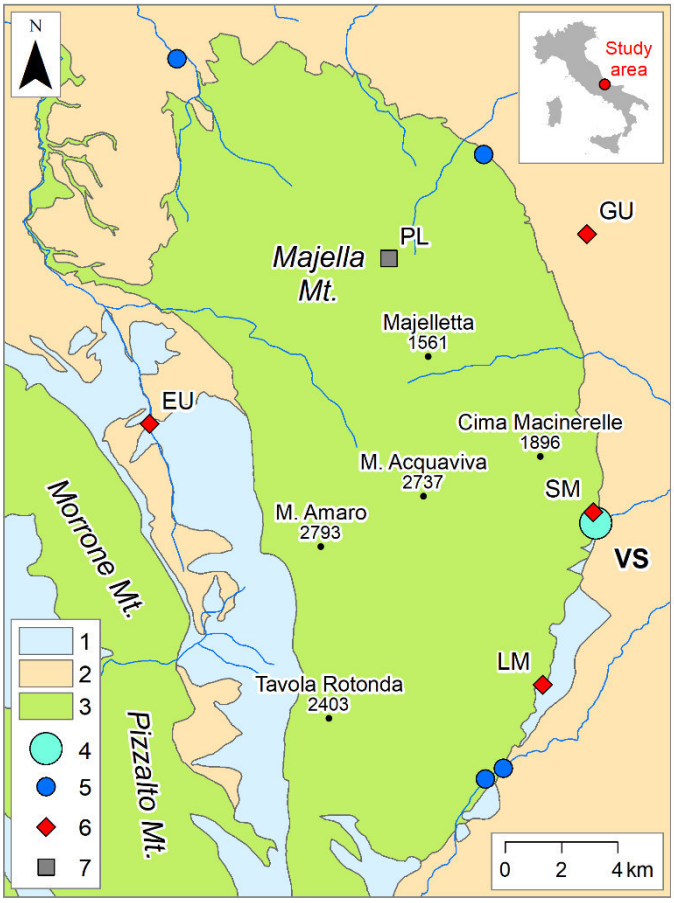

Fig. 1 Schematic hydro-geological map of the Majella massif. In legend: 1) continental deposits; 2) terrigenous deposits; 3) carbonate formations; 4) the Verde spring (VS); 5) other Majella aquifer basal springs; 6) rain gauges (LM, SM, GU, EU); 7) snow cover thickness measurement station (PL).

Dataset

In order to get a deeper insight on the Majella system groundwater flow, multiparameter daily time-series were considered, all related to the same time period between December 1st, 1997, and November 7th, 2002 (1803 days; about 5 years) and collected in different monitoring point all over the Majella massif (Fig. 1; Tab. 1).

The snow cover thickness (in cm; accuracy ±1 cm) was measured by means of a graduated scale by the Meteomont State Forestry Authority Service. The rainfall data (mm; accuracy ±0.1 mm), collected by automated rain gauges and representative of the overall rain precipitation on the Majella massif (Fig. 1), were provided by the Hydrographic Service of Abruzzo Region. The Verde spring discharge data is a sum of two different monitoring

158 (i.e. SASI SpA and Hydrographic Service of Abruzzo Region), performed by automated
159 water level stations with calibrated flow section (m^3/s; accuracy ±0.001 m^3/s). In addition,
160 for the Verde spring also the water electrical conductivity (µS/cm; accuracy ±0.01 µS/cm)
161 and temperature (°C; accuracy ±0.1° C) were measured by a physico-chemical
162 multiparameter probe connected with a data logger, located in the spring tapping (Nanni
163 and Rusi, 2003).
164 It is important to highlight that one of the discharge measurement points is located about
165 1800 m downstream of the spring tapping, thus partially influenced by runoff.
166
167 *Tab. 1 Monitoring points on the Majella massif. Sources: (1) Hydrographic Service of Abruzzo Region; (2)*
168 *(Nanni & Rusi, 2003) e Rusi (2000); (3) State Forestry Authority, Meteomont Service.*

Abbreviation	Location	Source	a.s.l.
PLS	Passo Lanciano snowmeter	(3)	1300
EUR	Sant'Eufemia a Majella rain gauge	(1)	810
LMR	Lama dei Peligni rain gauge	(1)	650
GUR	Guardiagrele rain gauge	(1)	577
SMR	Fara San Martino rain gauge	(1)	325
VSD	Verde spring discharge meter	(1)	410
VSEC	Verde spring electrical conductivity probe	(2)	410
VST	Verde spring temperature probe	(2)	410

169
170
171 *Autocorrelation Function*
172 The Autocorrelation Function (ACF) is a univariate analysis, that evaluates the linear
173 dependency of successive values of a single parameter in a selected time-series. For this
174 reason, the method describes the behavior of a selected time-series, that can be
175 considered random, systematic or mixed (Mangin, 1984; Benavente et al., 1985; Larocque
176 et al., 1998; Thanh Tam et al., 2004). To describe the behavior of considered time-series,
177 the autocorrelation curves and the decorrelation (i.e. ACF < 0.2) time lag are compared
178 (Mangin, 1984; Amraoui et al., 2003; Delbart et al., 2013). Usually, the random behaviour
179 is characterized by a fast decorrelation and short decorrelation lag times, while a

systematic behaviour by a gentle slope shape and long decorrelation lag times. In mixed conditions, the autocorrelation function is characterized by a multimodal curve. In this way, useful information about the aquifer systems can be obtained (Bouchaou et al., 2002; Duvert et al., 2015; Cai and Ofterdinger, 2016; Petalas, 2017).

The estimate of the k-th lag autocorrelation ($\hat{\mathrm{ACF}}(\mathrm{k})$) of a finite time-series of N observations is (Jenkins and Watts, 1968).

$$\hat{\mathrm{ACF}}(\mathrm{k}) \equiv \frac{\hat{\mathrm{c}}_{\mathrm{xx}}(\mathrm{k})}{\hat{\mathrm{c}}_{\mathrm{xx}}(0)} \equiv \frac{\hat{\mathrm{c}}_{\mathrm{xx}}(\mathrm{k})}{\hat{\sigma}_{\mathrm{x}}^{2}} \equiv \frac{\frac{1}{\mathrm{N}}\sum_{\mathrm{t}=1}^{\mathrm{N}-\mathrm{k}}(\mathrm{x_t}-\bar{\mathrm{x}})(\mathrm{x_{t+k}}-\bar{\mathrm{x}})}{\frac{1}{\mathrm{N}}\sum_{\mathrm{t}=1}^{\mathrm{N}}(\mathrm{x_t}-\bar{\mathrm{x}})^{2}} \qquad \mathrm{k} = 0, 1, 2, \ldots, \mathrm{K}$$

where $\hat{\mathrm{c}}_{\mathrm{xx}}(\mathrm{k})$ is the estimate of the auto-covariance, $\hat{\mathrm{c}}_{\mathrm{xx}}(0) \equiv \hat{\sigma}_{\mathrm{x}}^{2}$ is the estimate of the variance, $\bar{\mathrm{x}} = (\sum_{\mathrm{t}=1}^{\mathrm{N}} \mathrm{x_t})/\mathrm{N}$ is the mean of the time series and k is the number of the time series elements to be considered (usually a value not greater than N/4).

Cross-Correlation Function

The Cross-Correlation Function (CCF) is a bivariate analysis that describes the relationships between input and output, in terms of response time and the effective weight of input variation on the output behavior. Furthermore, the shape of the CCF function characterizes aquifers in terms of infiltration rate and travel time through the main infiltration pathways (Fiorillo and Doglioni, 2010), in terms of draining capacity and storage, identification of the main input parameter contribution (Mangin, 1984; Gárfias-Soliz et al., 2010; Lo Russo et al., 2014; Katsanou et al., 2015; Tonggang et al., 2016; Chiaudani et al., 2017; Hosseini et al., 2017).

It is shown in Jenkins and Watts (1968), that the estimate of the bivariate cross-correlation coefficient at lag k ($\hat{\mathrm{CCF}}(\mathrm{k})$) can be obtained by the following relation:

$$\hat{\mathrm{CCF}}(\mathrm{k}) \equiv \frac{\hat{\mathrm{c}}_{\mathrm{xy}}(\mathrm{k})}{\hat{\sigma}_{\mathrm{x}}(0)\cdot\hat{\sigma}_{\mathrm{y}}(0)} \equiv \frac{\frac{1}{\mathrm{N}}\sum_{\mathrm{t}=1}^{\mathrm{N}-\mathrm{k}}(\mathrm{x_t}-\bar{\mathrm{x}})(\mathrm{y_{t+k}}-\bar{\mathrm{y}})}{\frac{1}{\mathrm{N}}\sqrt{\sum_{\mathrm{t}=1}^{\mathrm{N}}(\mathrm{x_t}-\bar{\mathrm{x}})^{2}}\sqrt{\sum_{\mathrm{t}=1}^{\mathrm{N}}(\mathrm{y_t}-\bar{\mathrm{y}})^{2}}} \qquad \mathrm{k} = 0, 1, 2, \ldots, \mathrm{K}$$

Where (x_t, y_t) are the pairs of data variables (for example rainfall and spring discharge) to be compared to each other, while $\bar{x}$ and $\bar{y}$ are the means of the x and y series, respectively. The $\hat{CCF}$ values, to be acceptable, have to be characterized by the 95% confidence level ($p < 0.05$), that was tested by means of the Student's t-test (Seidenbecher et al., 2003), defined as:

$$t = \frac{r_{xy}(k)\sqrt{n-2}}{\sqrt{1-r_{xy}(k)}}$$

where, t is the t-value (equal to 1.645 for 95% significance level), and n is the number of observations of each time-series (i.e. 1803).

Seasonal-trend decomposition

Since in large aquifer systems the baseflow is predominant, the seasonal and long-term variation (non-casual component) can hide the effects of sporadic recharge events, especially when bivariate time-series analyses, such CCF, are applied. For this reason, analyzing residual changes is vital to avoid information loss.

In order to remove the periodical fluctuations (seasonal and multi-year cycles) and the trend components (i.e. non-casual long-term changes) in the selected time-series, the Census I method was chosen. The residual component obtained by this analysis represents the random short-term fluctuations, that are neither systematic nor predictable This approach is based on the assumption that an observed value x_t at time t in a time-series considered consists of four different components, combined to each other in an essentially additive model:

$$x_t = T_t \times C_t + S_t + \varepsilon_t$$

where: T_t is the trend component; S_t is the seasonal component (12-month period); C_t is the cyclical component that have usually a longer periodicity than the seasonal

223 component; ε_t is the random irregular component that is the most quickly changing. The
224 trend and cyclical components are customarily combined into a trend-cycle component
225 $T_t \times C_t$ (INSB, 1965; Béthoux et al., 1980; Makridakis et al., 1983; Makridakis and
226 Wheelwright, 1989; Polemio and Dragone 1999; HCSO, 2007).
227
228 **Results and discussion**
229 *Data description and basic statistics*
230 The multiparameter time-series considered in this research are shown in Fig. 2 and the
231 basic statistics concerning these datasets are presented in Tab. 2.
232 The snow cover thickness distribution (Fig. 2A) is marked by an intermittent behavior,
233 related to the alternation of snowy fall-winter periods and non-snowy periods. Its values
234 range from 0 cm to 210 cm, suggesting a high variable thickness. In addition, the low
235 mean and median values (25 cm and 0 cm, respectively), together with the 25th and 75th
236 percentiles (0 cm and 21 cm, respectively), suggest that the non-snowy days are
237 predominant in the time-series. The snowy periods are characterized by a rapid snow
238 cover increase and decrease, respectively during the snow accumulation and smelting.
239 The rainfall patterns (Fig. 2B) appear more random than the snow cover one. In fact, the
240 very small values of mean, median, 25th and 75th percentiles (Tab. 2), compared with the
241 maximum value (100.2 mm), confirm this non-systematic behavior. Although the rain
242 seems to fall during the whole years, the more intense and frequent events occur in the
243 early fall and in spring periods. Instead, stronger events, over about 50-60 mm, occur
244 rarely in the considered time period (Fig. 2B).
245 The Verde spring discharge (Fig. 2C) shows a seasonal behavior, characterized by values
246 ranging between 1.834 and 5.014 m^3/s. The highest values occur during and after the
247 snow melt (i.e. from April to July) and decrease following the typical spring regression
248 curve. Nevertheless, high discharge values were measured also before the snow

accumulation, especially when the measured yearly snow cover thickness was small (i.e. 1999 and 2000). This non-seasonal discharge pattern suggests that the Verde spring behavior is somehow influenced by rainfall when the snow cover is thin or absent, although its variability is very limited (Tab. 2). This little variation is likely attributable to deeper and/or slower flow paths that form the overall aquifer baseflow.

The same limited variability of discharge values is reflected in the electrical conductivity (EC) and temperature (T) statistics (Tab. 2). Analyzing the EC distribution (Fig. 2D), the lowest values coincide with the highest discharge values and increase gradually as the spring discharge decreases, reaching the lowest values during the fall period. This relation with the discharge is due to the recharge of the aquifer system by waters poor in total dissolved solids, even though they contribute to the whole water volume with a relative smaller amount than the one of the baseflow. In addition, EC seems to decrease sharply during the intense and concentrated rainy periods. This effect lasts for few days. The same dependency on discharge fluctuations is shown by T (Fig. 2E), although varying in the range 8.4-8.6° C (Tab. 2). This very limited variability can be attributable to slight differences between recharge water and groundwater temperature as well as to the relatively small volume of colder water feeding the aquifer, respect to the stored volume.

The Skewness (S) and Kurtosis (K) values are always different from the Normal, or Gaussian, distribution that has S = 0 e K = 3 (Tab. 2). When S and K values are positive, it means that the time-series are characterized by most of the values varying slightly around the median, that is always minor that the mean, and by few out-layers close the maximum value. This distribution suggests the coexistence of more than one condition influencing the parameter fluctuation, such as the alternation of snowy and non-snowy periods as in snow cover thickness or intermittent recharge periods as in spring discharge, or the random behavior as in rainfall time-series. EC and T are the only exceptions, since their S

274 and K values are similar to the Normal ones because of the limited effect of the input
275 variables.

276 *Tab. 2 Basic statistics of the considered multiparameter time-series.*

Parameter	Unit	Count	Mean	Median	Min	25^{th}	75^{th}	Max	S	K
PLS	cm	1803	25	0	0	0	21	210	1.8	2.2
EUR	mm	1803	3.3	0	0	0	1.6	100.2	4.6	28.2
LMR	mm	1803	2.1	0	0	0	1.0	77.1	5.1	38.5
GUR	mm	1803	2.3	0	0	0	1.2	72.4	4.9	31.9
SMR	mm	1803	2.2	0	0	0	1.6	74.3	5.2	38.3
VSD	m^3/s	1803	2.797	2.714	1.834	2.562	2.994	5.014	1.1	2.3
VSEC	µS/cm	1803	251.63	251.99	230.58	249.33	254.52	261.15	-0.7	1.2
VST	° C	1803	8.5	8.5	8.4	8.5	8.5	8.6	-0.5	3.7

277

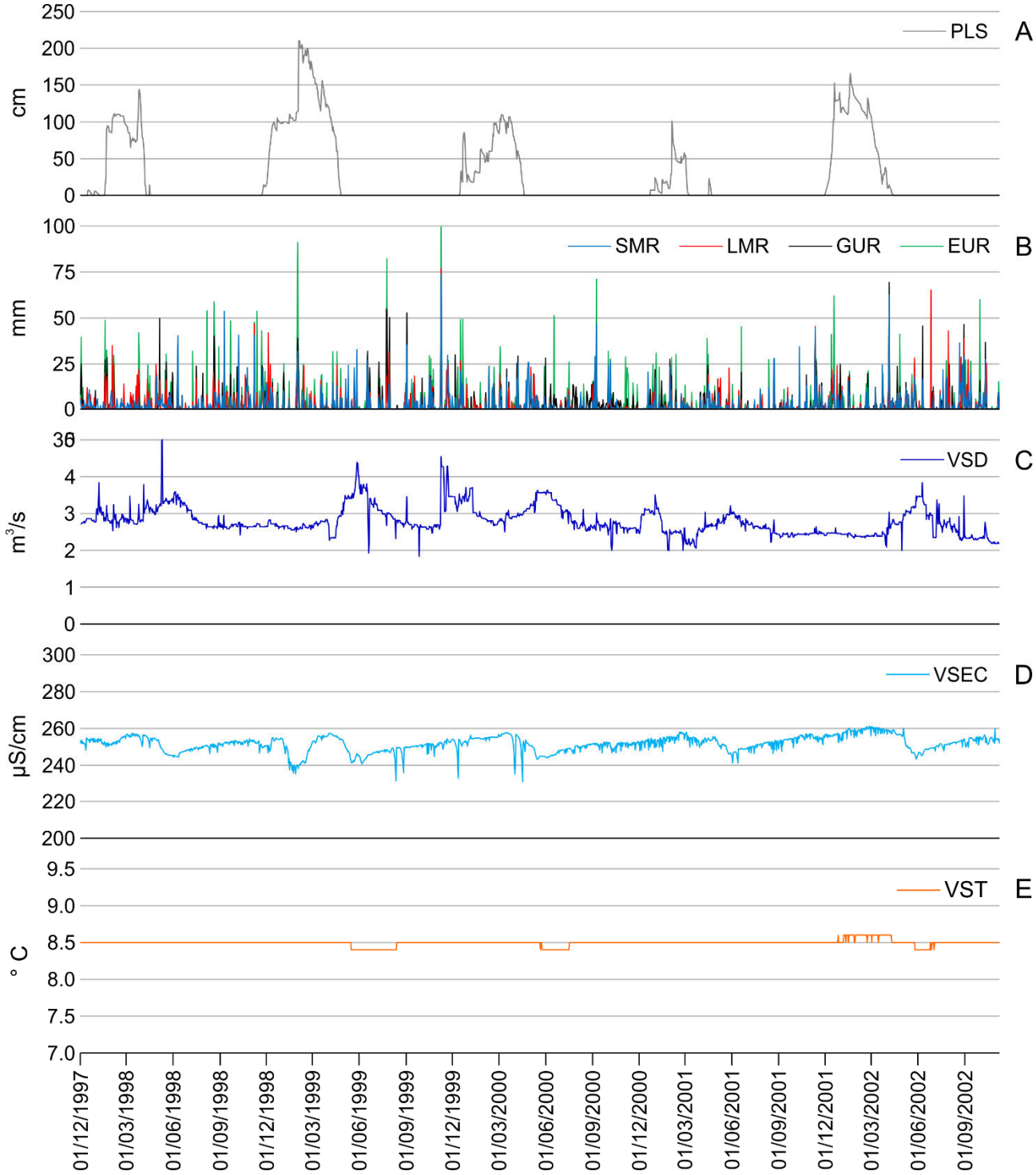

Fig. 2 The multiparameter time-series considered in this study and related to the monitoring points represented in Fig. 1 and Tab. 1. A) Snow cover thickness; B) rainfall; C) spring discharge; D) spring electrical conductivity; E) spring temperature.

The mean daily standardized year-type of the 1998-2001 period (Fig. 3) summarizes the main features of the considered time-series. In particular, the snow covers the recharge areas from December to April, while rainfall confirms its random behavior during the whole

year. Intense rainfall events are more frequent in November and April. The Verde spring discharge, instead, reaches its highest values in June, decreasing until October. In November, random discharge increases occur. Concerning EC and T, the lower values clearly occur when the spring discharge is high because of the recharge.

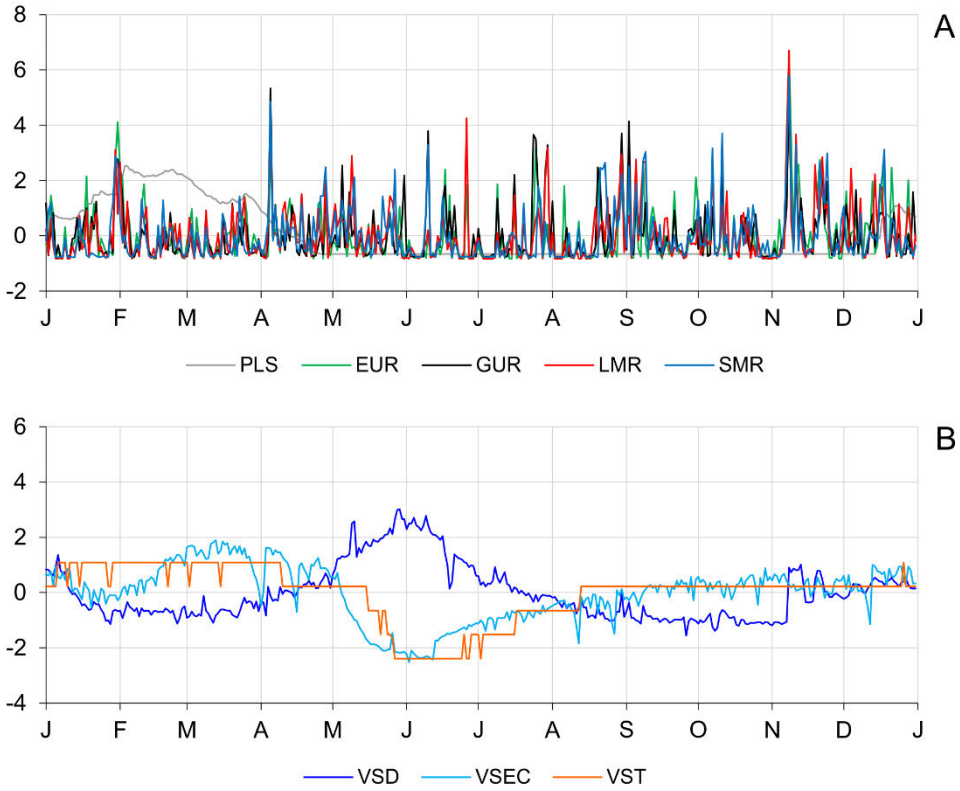

Fig. 3 The mean daily standardized year-type (1998-2001 period) of input (A) and output (B) parameters, described in Tab. 1.

Autocorrelation

The ACF results, represented in Fig. 4, shows that the rainfall time-series sharply decorrelate because of their random behavior. Contrariwise, the snow cover thickness decorrelates regularly in about 60 days. This ACF shape is related to the regular trend of the snow cover thickness time-series. The same regular behavior is reflected in the spring discharge, EC and T curves, that decorrelate in about 50-60 days. Nevertheless, the

spring discharge and EC decorrelation curves present a sharp decrease of ACF in the first 10 days, similar to the rainfall decorrelation. This trend is likely attributable to instantaneous variations caused by the occasional recharge events that are due to intense and concentrated rainfall. For this reason, the variability of the spring discharge and EC time-series can be accounted by the combined effect of both rainfall (i.e. random component) and snowmelt (i.e. systematic component) recharge. In contrast, the T curve does not seem to be affected probably because the temperature is almost steady as a result of the slight difference between the infiltrating water and the groundwater volume stored within the Majella aquifer system (i.e. baseflow).

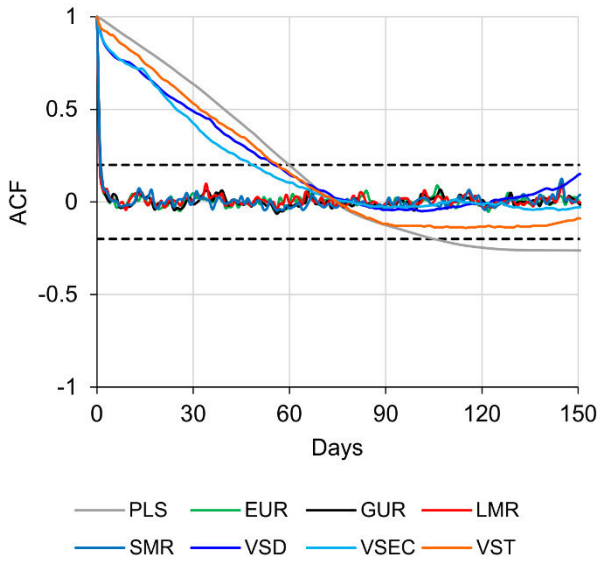

Fig. 4 ACF curves of the considered time-series. The dashed lines indicate the positive and negative confidence levels.

Raw data cross-correlations

In order to examine the effect of recharge on the Verde spring parameters, the Cross-Correlation Function (CCF) was applied to both the raw and residual time-series. Fig. 5 shows the results of CCF between raw input and output datasets. At first sight, the CCF

values describing the snow cover thickness-spring parameters relationship are an order of magnitude higher than the ones related to the rainfall-spring parameters relationship. This noticeable gap is attributable to the difference in water volume infiltrating during and after snowmelt and after rainfall events. In fact, the Majella aquifer system recharge is mainly due to the snow cover that accumulates, during the fall-winter period (i.e. from November to February), and then melts, during the spring period (i.e. March-April). Rainfall events, even intense and widespread, supply little water to the aquifer with respect to the water volumes accumulated in the form of snow, in the recharge areas.

Analyzing in detail, the CCF between the snow cover thickness (PLS) and the spring discharge (VSD), represented in Fig. 5A, shows the maximum positive correlation (0.54) with a time lag equal to about 110 days, even though the curve appears very smooth with correlation values above the significance level in the range 65-145 days. As expected, the CCFs between the snow cover thickness and the spring electrical conductivity (VSEC) and temperature (VST) are characterized by evident negative values (-0.45 and -0.59, respectively; Fig. 5B and 5C), because of the mixing between the groundwater already stored in the aquifer (i.e. baseflow) and the recharge water, and the resulting dilution effect. Nevertheless, the corresponding time lags are in both cases about 135 days, that is about 25 days later that the maximum time lag of the PLS-VSD (cover thickness vs spring discharge) cross-correlation. As for the PLS-VSD, the CCF curves are very smooth and wide. The apparent discrepancy in the time lags for the different spring parameter CCFs can be explained by a delay in the diluted groundwater arrival at the Verde spring. Thus, the PLS-VSD time lag includes the snow cover accumulation, the snow melting, the snowmelt infiltration, and the first arrival of large water volumes to the water table (i.e. pressure transfer, Nanni and Rusi, 2003; Aquilina et al., 2006; Di Lorenzo et al., 2018), that alters the hydraulic head distribution in the aquifer and causes the spring discharge to increase rapidly. Within the following 25 days, the recharge water mixes with the stored

347 groundwater and moves toward the spring. The coexistence of several infiltration modes
348 (i.e. flow paths in the unsaturated zone), characterized by different sizes and hydraulic
349 conductivities, accounts for the smoothed and widened curves. In addition, the significative
350 correlations at short time lags (negative value for snow cover thickness-spring discharge
351 cross-correlation, and positive values for snow cover thickness-electrical conductivity and
352 temperature) can be attributed to the simultaneous coexistence of the snowfall
353 accumulation in the recharge areas and the spring recession, in the fall-winter period (Fig.
354 3).
355 Concerning the CCFs between rainfall (EUR, GUR; LMR, and SMR) and the Verde spring
356 discharge (VSD), the CCF curves (Fig. 5D) are very irregular and the highest values (up to
357 0.08) has a time lag equal to about 110 days, that is comparable with the one obtained in
358 the PLS-VSD cross-correlation. These coherent time lag can be explained by the effect of
359 the rainfall events in the March-April period that, together with the increasing air
360 temperature, favor the snow melting and the subsequent snowmelt infiltration. Besides the
361 longer time lag, the rainfall vs. spring discharge CCFs points out several significative
362 positive peaks (up to 0.09), characterized by time lags shorter than 50 days (i.e. 0, 5, 13,
363 22, 35, and 45 days). However, the instantaneous one (i.e. 0-day time lag) must be
364 excluded from the analysis because it is likely due to the runoff component affecting the
365 spring discharge measurement in the stream section between the spring tapping and the
366 discharge gauging station. The other short time lags are probably attributable to different
367 flow paths, that contribute, even slightly, to the Verde spring discharge variations. The
368 CCFs between rainfall and the Verde spring electrical conductivity (Fig. 5E) and
369 temperature (Fig. 5F) have unclear results, especially for the rainfall-spring temperature
370 one.

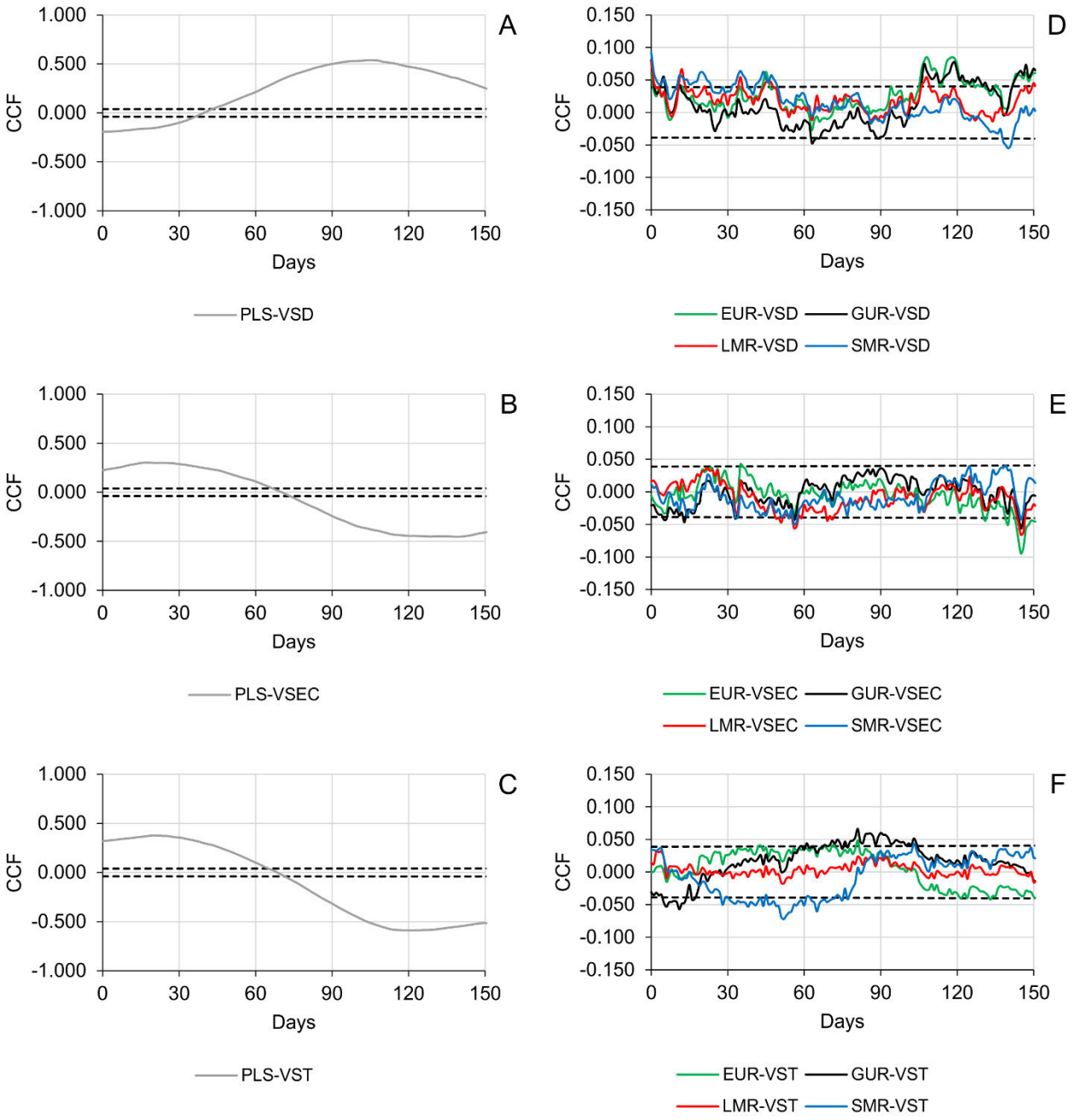

Fig. 5 Raw time-series CCFs between the snow cover thickness and the Verde spring parameters (A, B, and C), and between rainfall and Verde spring parameters (D, E, and F). The dashed lines indicate the positive and negative confidence levels.

Raw rainfall-residual spring parameter cross-correlations

Since the low raw data CCF values confirm that the rainwater volume contribution to the Majella aquifer recharge is very limited and the overall rainfall is supposed to affect only the residual non-systematic behavior of the Verde spring parameters, the CCF was

applied to the residual spring discharge (rVSD), electrical conductivity (rVSEC) and temperature (rVST) time-series, considering the raw rainfall time-series as input. The results of these analyses are represented in Fig. 6. This kind of analysis allowed to improve the resolution and to better highlight the significative peaks not clearly visible in Fig. 5. In addition, grouping the CCFs by specific rain gauge to compare the rainfall time-series effect on the different residual spring parameter behavior, hydrodynamic considerations can be pointed out, in terms of recharge modes.

The raw rainfall-rVSD cross-correlations (Fig. 6) show clear peaks characterized by response times equal to 5 days (peak I), 13 days (peak II), 22 days (peak III), 35 days (peak IV), and 45 days (peak V). The CCFs between raw rainfall and residual spring physico-chemical parameters exhibit a similar pattern of the significative negative peaks, but the response times so not always coincide. In detail, the peaks I and II, detected in the raw rainfall-rVSD curves, have delays (response times equal to 7 and 15 days, respectively) in the CCFs with rVSEC and rVST of 2 days. The peak III of the raw rainfall-rVSD is present only once with a low CCF value (0.038, barely significative) and does not show negative peaks in the CCFs with rVSEC and rVST. The peak IV is characterized by identical response times for both raw rainfall-rVSD and raw rainfall-rVSEC, equal to 35 days. The CCFs with the rVST does not show any significative negative peak. Finally, the peak V of the raw rainfall-rVSD curves is characterized by a response time of 45 days, but the CCFs with the rVSEC is delayed by 11 days. As for peak IV, even in this case, the CCFs between raw rainfall and rVST does not show any significative negative peak.

This complex and heterogeneous framework suggests that, when a rainfall event occurs, rainwater reaches the Verde spring through different flow paths in both unsaturated and saturated zones. Once rainwater reaches the saturated zones, the hydraulic head raises instantaneously and causes a rapid discharge increase (i.e. pressure transfer). This water then mixes with the groundwater already stored in the Majella aquifer, slightly diluting it.

Later, the diluted groundwater reaches the Verde spring in a given time period (i.e. transport period), that depends on the distance from the spring and the overall hydraulic conductivity of the aquifer in the saturated zone. Thus, the more the infiltrating rainwater volume is large, the more the diluting effect due only to the rainfall recharge is evident, since even the aquifer dispersivity tends to attenuate further this effect during the groundwater transport period.

Based on these considerations, the peaks highlighted by the raw rainfall-residual spring parameter CCFs can likely correspond to different recharge modes, that differ from one another in infiltrating water volume amount, size (i.e. length and width) and hydraulic conductivity of fractures and/or karst conduits, and distance from the Verde spring. As a result, the peaks that are characterized by a delayed physico-chemical response time (i.e. peaks I, II, and V) can be attributable to large karst conduits or intensely fractured zones that bring significant amounts of water through the unsaturated zone into the saturated one (Fig. 7). This water then mixes with the groundwater already stored in the aquifer and moves downstream, reaching the spring within the delay between the discharge and the physico-chemical parameter response times. Furthermore, the differences in the spring recharge response depend on the travel time in the unsaturated zone that is related to the length and/or the hydraulic conductivity of the corresponding flow paths. On the other hand, the delay between the discharge and the physico-chemical parameter response is a function of the mixing and the advective-dispersive transport of mixed groundwater toward the spring. The overall delaying effect due to these processes, in turn, depends on the distance from the spring and the aquifer hydraulic conductivity. Contrariwise, the peak III, that does not show negative peaks in the CCFs with the spring physico-chemical parameters, can be interpreted as a narrow conduit or a slightly fractured zone, that brings to the saturated zone a small amount of rainwater cannot alter significantly the groundwater physico-chemical parameters. For this reason, only the travel time toward the

saturated zone and the following pressure transfer are clearly detectable (i.e. 22 days), that can be attributable to an intermediate-length flow path in the unsaturated zone (Fig. 7). Finally, the infiltration through the dense fracture network, taking place within the bulk rock mass of the Majella massif, can account for the peak IV, that characterized by a simultaneous alteration of the spring discharge and physico-chemical parameters. As a matter of fact, the slow downward movement in these conditions limits the effect of the pressure transfer on the spring discharge and favors the mixing. For this reason, the simultaneous response times (i.e. 35 days) include both the travel time within the unsaturated zone and the mixing and the advective-dispersive transport of mixed groundwater toward the spring (Fig. 7).

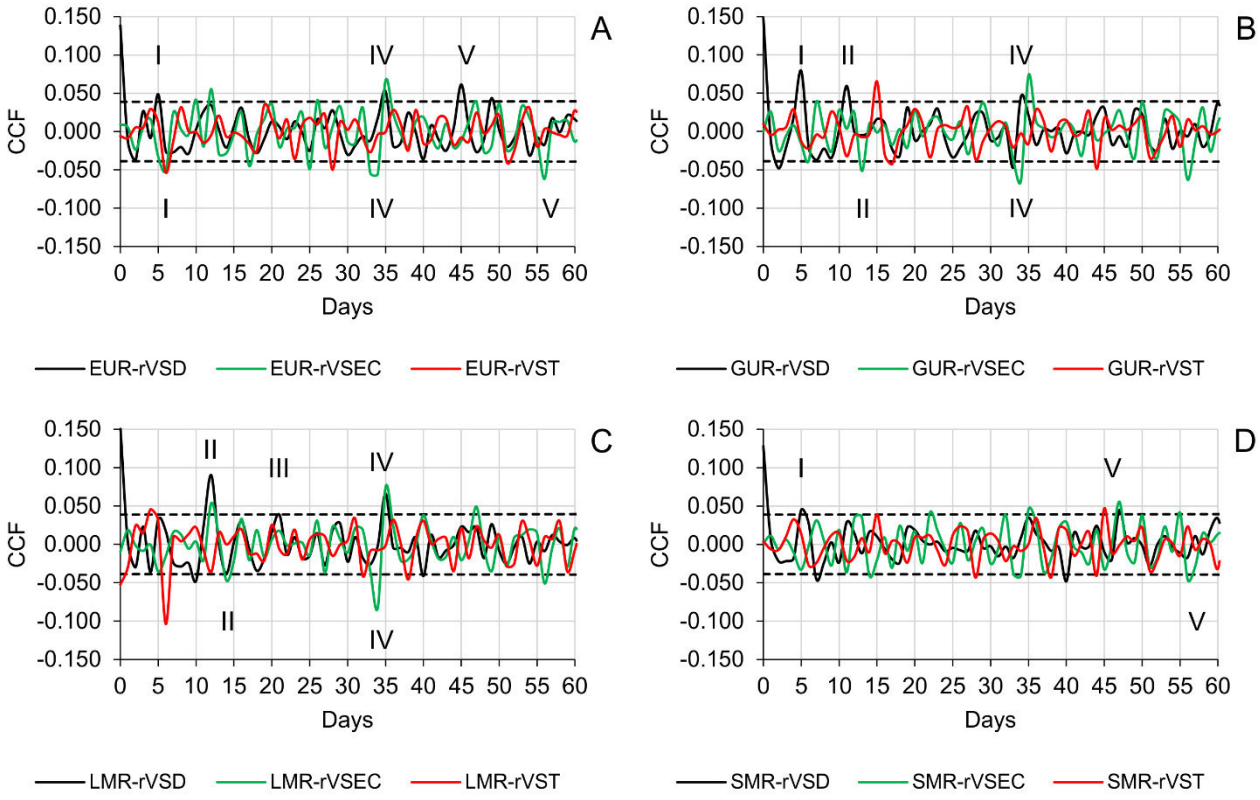

Fig. 6 Raw rainfall-residual spring parameter CCF curves. A) EUR-residual VS parameters; (B) GUR-residual VS parameters; C) LMR- residual VS parameters; D) SMR- residual VS parameters. The Roman numerals in Fig. 6 represent different recharge modes. The dashed lines indicate the positive and negative confidence levels.

The Verde spring conceptual model

The results obtained analyzing the multiparameter time-series allowed to get a deeper insight into the Majella aquifer system recharge and unsaturated-saturated flow. In particular, a refined conceptual model of the role of each inflow on the overall renewable groundwater volume of the Majella aquifer system and of the different modes (i.e. unsaturated-saturated) by which the recharge water reaches the Verde spring was defined (Fig. 7).

The snowmelt represents the major inflow of the aquifer system (Fig. 7A), because of the huge snow volume that accumulates in the recharge areas, during the fall-winter period, and melts, during the spring period. The snow cover melting, favored also by intense rainfall, leaks slowly large amount of water into the aquifer, all over the recharge areas. The large snowmelt volume inflow, due to the combination of a multitude of different recharge modes, creates significative modifications to the spring discharge (about +1.5 m^3/s), electrical conductivity (about -30 µS/cm) and temperature (about -0.1° C), in terms of groundwater volume increase and dilution (Fig. 2). In addition, the delayed response times of the CCFs with the physico-chemical parameters (Fig. 5) highlighted that the diluted groundwater takes an average of 25 days to reach the Verde spring. Nevertheless, the steady slow snowmelt inflow tends to saturate a large portion of the voids present in the unsaturated zone (i.e. karst conduits, large fractures and dense fracture network). For this reason, distinguishing the single snowmelt recharge modes was not possible, as pointed out by the CCFs between the snow cover thickness and the Verde spring parameters that show very smoothed and wide response curves for all the spring parameters (Fig. 5).

Concerning the rainfall contribution, the very low CCFs values, considering both raw (Fig. 5) and residual (Fig. 6) spring parameter time-series, confirmed that the rainfall volume inflow represents only a limited amount of the overall Majella aquifer recharge. However,

477 the transient behavior of the rainfall inflow allowed to identify different recharge modes
478 (Fig. 6 and 7B), that are fully or in part activated during intense rainfall events. These
479 recharge modes depend on several flow paths in the unsaturated zone that are
480 characterized by different water volumes brought downward, sizes (i.e. length and width),
481 hydraulic conductivities, and distances from the Verde spring (Fig. 7B). Each of these
482 recharge modes affects the spring parameter behaviors differently. Although their
483 influence is generally limited in duration, sharp and significative discharge increases (up to
484 about +0.7 m^3/s) and electrical conductivity decreases (up to about -20 µS/cm) can occur
485 (Fig. 2). Nevertheless, the spring temperature is not sensitive to rainfall inflow because of
486 the rainwater is affected by the air temperature variations, thus a clear temperature
487 decrease is not detectable, as for the snowmelt inflow (Fig. 7).
488

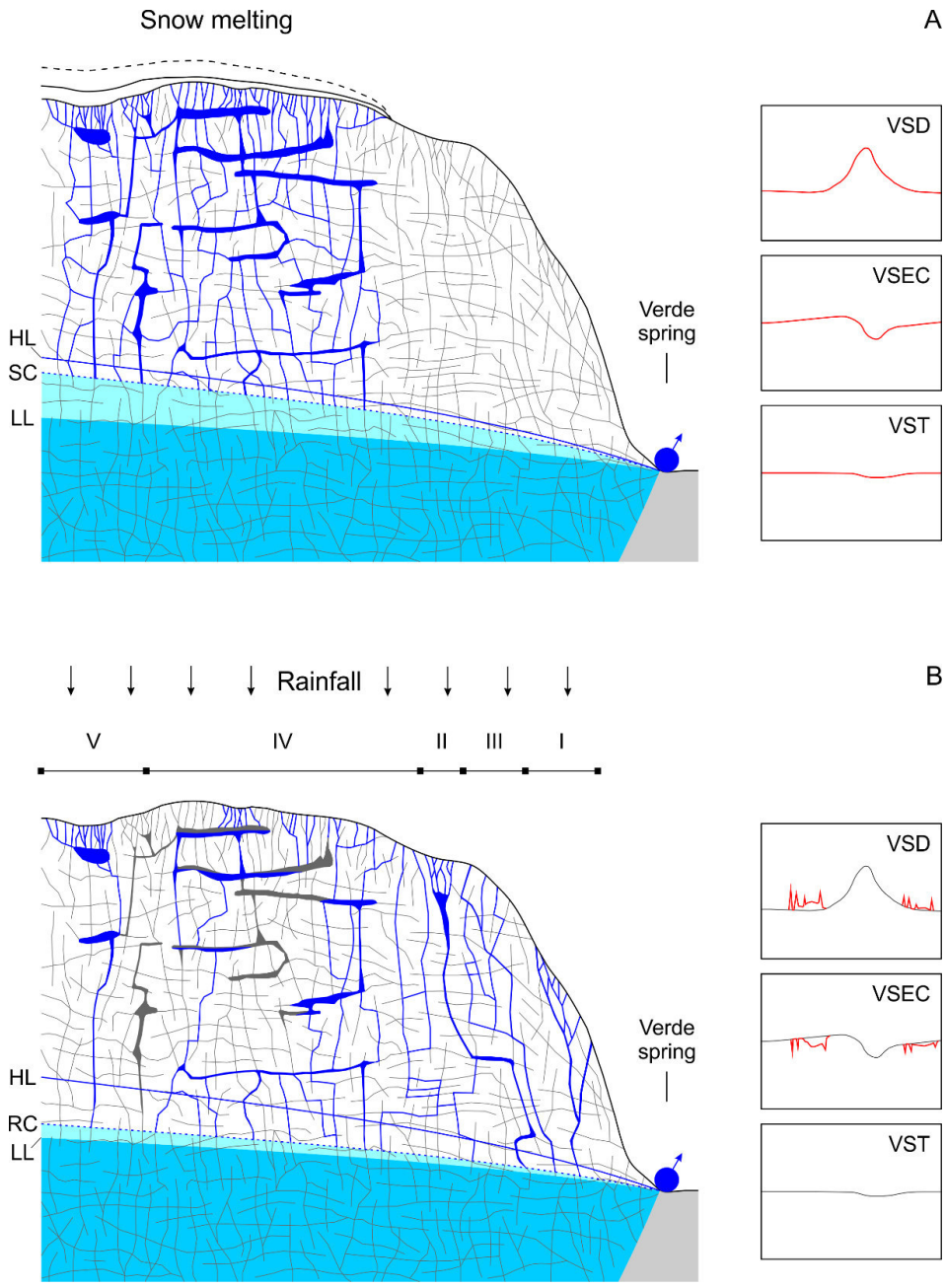

Fig. 7 Simplified conceptual model of the snowmelt (A) and rainfall (B) inflow contributions to the overall recharge of the Majella aquifer system (HL: higher level; SC: snowmelt contribution; RC: rainfall contribution; LL: lower level). In red, each inflow contribution to the Verde spring parameter behavior. The Roman numerals refer to the different recharge modes identified in Fig. 6.

Conclusions

This study demonstrated that the multiparameter hydrodynamic and hydrochemical time-series analyses, related to heterogenous fractured and/or partially karst aquifer systems, can provide more detailed information about the groundwater flow and the recharge

modes, without using tracer tests. Although they are more precise and the used tracers non-toxic, their implementation is often difficult because of the logistic conditions and the environmental restrictions, especially when the aquifer systems are wide, and the related groundwater exploited for drinking purposes. In addition, the tracer tests are not reliable when the aquifer systems are wide, and the karstic features are scarce or absent.

As a matter of fact, a preliminary conceptual model of the groundwater flow and the different inflows, that recharge the aquifer and affect the spring parameter behavior, is required.

In the Majella massif, the results obtained clearly demonstrated that the snowmelt contribution is predominant with respect to the rainfall one. The travel times in the unsaturated and saturated zones of the water moving toward the Verde spring and the aquifer recharge modes depend on the different inflows (i.e. snowmelt and rainfall), their distribution in the recharge areas, their intensity and distribution in time. In detail, the multiparameter time-series analyses allowed to identify several recharge modes related to different flow paths, that are characterized by different features (i.e. size, hydraulic conductivity and distance from the spring), in both the unsaturated and saturated zones.

The level of detail obtained by the multiparameter time-series analyses is high, although below the one provided by tracer tests. In fact, this methodological approach allowed to account for small changes in the spring parameters, such as the electrical conductivity (about ± 15 μS/cm) and temperature (about ± 0.1° C). In general, these small variations are considered meaningless.

As a result, the multiparameter time-series analytical approach, useful for the Majella aquifer system case study, can be applied to other large heterogenous fractured and/or partially karst aquifer systems worldwide, where the recharge is due to both rainfall and snowmelt.

526 **Acknowledgement**

527 The authors would like to thank Dr. Alain D'Ettorre for his contribution, the Hydrographic
528 Service of Abruzzo Region for the rainfall and spring discharge data, the Meteomont State
529 Forestry Authority Service for the snow cover thickness data, and the SASI SpA for the
530 information about the Verde spring management and exploitation.

531

532 **References**

533 Amraoui, F., Razack, M., Bouchaou, L., 2003. Turbidity dynamics in karstic systems.
534 Example of Ribaa and Bittit springs in the Middle Atlas (Morocco). Hydrol. Sci. J. 48 (6),
535 971-984. https://doi.org/10.1623/hysj.48.6.971.51418

536 Aquilina, L., Ladouche, B., Dörfliger, N., 2006. Water storage and transfer in the epikarst of
537 karstic systems during high flow periods. J. Hydrol. 327(3–4), 472-485.
538 https://doi.org/10.1016/j.jhydrol.2005.11.054

539 Başağaoğlu, H., Gergen, L., Green, R. T., 2015. Assessing the Effects of Epikarst on
540 Groundwater Recharge and Regional Fast-Flow Pathways in a Karstic Aquifer via
541 Impulse-Response Functions. J. Hydrol. Engineering. 20(11), 04015021(1-13).
542 https://doi.org/10.1061/(ASCE)HE.1943-5584.0001183

543 Bayard, D., Stahli, M., Parriaux, A., Fluhler, H., 2005. The influence of seasonally frozen
544 soil on the snowmelt runoff at two Alpine sites in southern Switzerland. J. Hydrol. 309 (1),
545 66–84. https://doi.org/10.1016/j.jhydrol.2004.11.012

546 Benavente, J., Pulido-Bosch, A., Mangin, A., 1985. Application of correlation and spectral
547 procedures to the study of the discharge in a karstic system (Eastern Spain). Proceedings
548 of the Karst Water Resources Symposium, Ankara-Antalya, Turkey, IAHS, 161, 67-75.

549 Bethoux, N., Etienne, M., Ibanez, F., Rapaire, J.L. 1980. Spécificités hydrologiques des
550 zones littorales. Analyse chronologique par la méthode CENSUS II et estimation des

551 échanges océan-atmosphère appliquée à la baie de Villefranche sur Mer, Annales de
552 l'Institut Océanographique. 56, 81-95.
553 Bouchaou, L., Mangin, A., Chauve, P., 2002. Turbidity mechanism of water from a karstic
554 spring: example of the Ain Asserdoune spring (Beni Mellal Atlas, Morocco). J. Hydrol. 265,
555 34–42. https://doi.org/10.1016/S0022-1694(02)00098-7
556 Box, G.E.P., Jenkins, G.M., Reinsel, G.C., 1994. Time Series Analysis: Forecasting and
557 Control, 3rd ed.; Prentice Hall: Englewood Cliffs, NJ, USA.
558 Brutsaert, W., Nieber, J. L., 1977. Regionalized drought flow hydrographs from a mature
559 glaciated plateau. Water Resour. Res. 13(3), 637–643.
560 https://doi.org/10.1029/WR013i003p00637
561 Cai, Z., Ofterdinger, U., 2016. Analysis of groundwater-level response to rainfall and
562 recharge estimates in fractured hard rock aquifers, NW Ireland. J. Hydrol. 535, 71-84.
563 https://doi.org/10.1016/j.jhydrol.2016.01.066
564 Calamita, F., Scisciani, V., Montefalcone, R., Paltrinieri, W., Pizzi, A., 2002. L'ereditarietà
565 del paleomargine dell'Adria nella geometria del sistema orogenico centro-appenninico:
566 l'area abruzzese esterna [The role of the Adria paleomargin on the Central Apennines
567 thrust system geometry: the outer Abruzzi area]. Mem. Soc. Geol. It. 57, 355-368.
568 Celico, P., 1978. Schema idrogeologico dell'Appennino carbonatico centro meridionale
569 [Hydrogeological scheme of the carbonatic central-southern Apennine]. Mem. e Note Ist.
570 Geol. Appl. Univ. Napoli, 14, 5-97
571 Chiaudani, A., Di Curzio, D., Palmucci, W., Pasculli, A., Polemio, M., Rusi, S., 2017.
572 Statistical and Fractal Approaches on Long Time-Series to Surface-Water/Groundwater
573 Relationship Assessment: A Central Italy Alluvial Plain Case Study. Water, 9, 850.
574 https://doi.org/10.3390/w9110850
575 Crescenti, U., Crostella, A., Donzelli, G., Raffi, G., 1969. Stratigrafia della serie calcarea
576 dal Lias al Miocene nella regione marchigiano abruzzese (parte II: litostratigrafia,

577 biostratigrafia, paleogeografia) [Stratigraphy of the calcareous series from the Lias to the
578 Miocene in the Abruzzo and Marche regions]. Mem. Soc. Geol. It., 8, 343-420.
579 Daher, W., Pistre, S., Kneppers, A., Bakalowicz, M., Najem, W., 2011. Karst and artificial
580 recharge: Theoretical and practical problems. A preliminary approach to artificial recharge
581 assessment. J. Hydrol. 408(3–4), 189–202. https://doi.org/10.1016/j.jhydrol.2011.07.017
582 Delbart, C., Valdes, D., Barbecot, F., Tognelli, A., Richon, P., Couchoux, L., 2013.
583 Temporal variability of karst aquifer response time established by the sliding-windows
584 cross-correlation method. J. Hydrol. 511, 580-588.
585 https://doi.org/10.1016/j.jhydrol.2014.02.008
586 Di Curzio, D., Palmucci, W., Rusi, S., Signanini, P., 2016. Evaluation of processes
587 controlling Fe and Mn contamination in the San Pedro Sula porous aquifer (North Western
588 Honduras). Rend. Online Soc. Geol. It. 41, 42-45. https://doi.org/10.3301/ROL.2016.88
589 Di Lorenzo, T., Cipriani, D., Fiasca, B., Rusi, S., Galassi, D.M.P., 2018. Groundwater drift
590 monitoring as a tool to assess the spatial distribution of groundwater species into karst
591 aquifers. Hydrobiologia. 813, 137-156. https://doi.org/10.1007/s10750-018-3515-1.
592 Dragoni, W., Sukhija, B.S., 2008. Climate Change and Groundwater. Geological Society,
593 London, Special Publications Volume 288.
594 http://sp.lyellcollection.org/content/specpubgsl/288/1/local/front-matter.pdf
595 Duvert, C., Jourde, H., Raiber, M., Cox, M.E., 2015. Correlation and spectral analyses to
596 assess the response of a shallow aquifer to low and high frequency rainfall fluctuations. J.
597 Hydrol. 527, 894–907. https://doi.org/10.1016/j.jhydrol.2015.05.054
598 Fiorillo, F., 2009. Spring hydrographs as indicators of droughts in a karst environment. J.
599 Hydrol. 373(3-4), 290-301. https://doi.org/10.1016/j.jhydrol.2009.04.034
600 Fiorillo, F., Doglioni, A., 2010. The relation between karst spring discharge and rainfall by
601 cross-correlation analysis (Campania, southern Italy). Hydrogeol J. 18, 1881–1895.
602 https://doi.org/10.1007/s10040-010-0666-1

603 Fiorillo, F., 2011. Tank-reservoir drainage as a simulation of the recession limb of karst
604 spring hydrographs. Hydrogeol. J. 19(5), 1009-1019. https://doi.org/10.1007/s10040-011-
605 0737-y
606 Fiorillo, F., Petitta, M., Preziosi, E., Rusi, S., Esposito, L., Tallini, M., 2015. Long-term
607 trend and fluctuations of karst spring discharge in a Mediterranean area (central-southern
608 Italy). Environ. Earth Sci. 74, 153-172. https://doi.org/10.1007/s12665-014-3946-6
609 Galleani, L., Vigna, B., Banzato, C., Russo, S.L., 2011. Validation of a Vulnerability
610 Estimator for Spring Protection Areas: The VESPA index. J. Hydrol. 396(3-4), 233–245.
611 https://doi.org/10.1016/j.jhydrol.2010.11.012
612 Gárfias-Soliz, J., Llanos-Acebo, H., Martel, R., 2010. Time series and stochastic analyses
613 to study the hydrodynamic characteristics of karstic aquifers. Hydrol. Process. 24, 300-
614 316. https://doi.org/10.1002/hyp.7487
615 Ghisetti, F., Vezzani, L. (1997) Interfering paths of deformation and development of arcs in
616 the fold-and-thrust belt of the central Apennines (Italy). Tectonics. 16, 523-536.
617 HCSO (Hungarian Central Statistical Office), 2007. Seasonal Adjustment Methods and
618 Practices. European Commission Grant 10300.2005.021-2005.709. Final Version 3.1., 127
619 pp.
620 Hosseini, S.M., Ataie-Ashtiani, B., Simmons, C.T., 2017. Spring hydrograph simulation of
621 karstic aquifers: Impacts of variable recharge area, intermediate storage and memory
622 effects. Journal of Hydrology. 552, 225-240. https://doi.org/10.1016/j.jhydrol.2017.06.018
623 INSB (Institut National de Statistique de Belgique), 1965. Décomposition des séries
624 chronologiques en leurs composantes suivant différentes méthodes. Etudes statistiques et
625 économétriques. Bull. Stat. INS, 10:1449-1524.
626 Jenkins, G.M., Watts, D.G., 1968. Spectral Analysis and its Applications. Holden Day, San
627 Francisco, CA.

628 Jukić, D., Denić-Jukić, V., 2015. Investigating relationships between rainfall and karst-
629 spring discharge by higher-order partial correlation functions. J. Hydrol. 530, 24–36.
630 https://doi.org/10.1016/j.jhydrol.2015.09.045
631 Katsanou, K., Lambrakis, N., Tayfur, G., 2015. Describing the Karst Evolution by the
632 Exploitation of Hydrologic Time-Series Data. Water Resour. Manage. 29, 3131-3147.
633 https://doi.org/10.1007/s11269-015-0987-x
634 Kresic, N., Stevanovic, Z., 2009. Groundwater Hydrology of Springs: Engineering, Theory,
635 Management and Sustainability, Butterworth-Heinemann, Oxford.
636 Larocque, M., Mangin, A., Razack, M., Banton, O., 1998. Contribution of correlation and
637 spectral analyses to the regional study of a karst aquifer (Charente, France). J. Hydrol.
638 205, 217-231. https://doi.org/10.1016/S0022-1694(97)00155-8
639 Larocque, M., Banton, O., Razack, M., 2000. Transient-state history matching of a karst
640 aquifer ground water flow model. Groundwater. 38(6), 939-946.
641 https://doi.org/10.1111/j.1745-6584.2000.tb00694.x
642 Liberatoscioli, E., Boscaino, G., Agostini, S., Garzarella, A., Patacca Scandone, E., 2018.
643 The Majella National Park: An Aspiring UNESCO Geopark. Geosciences. 8, 256.
644 https://doi.org/10.3390/geosciences8070256
645 Liu, L., Shu, L., Chen, X., Wang, E., Oromo, T., 2010. Rainfall-driven spring hydrograph
646 modeling in a karstic water system, southwestern China. Water Resour. Manage., 24(11),
647 2689–2701. https://doi.org/10.1007/s11269-009-9574-3
648 Lo Russo, S., Amanzio, G., Ghione, R., 2014. Recession hydrographs and time series
649 analysis of springs monitoring data: application on porous and shallow aquifers in
650 mountain areas (Aosta Valley). Environ. Earth Sci., 73, 7415-7434.
651 https://doi.org/10.1007/s12665-014-3916-z
652 Makridakis, S. G., Wheelwright, S. C., McGee, V. E., 1983. Forecasting: Methods and
653 applications, 2nd ed.; New York Wiley: New York, NY.

654 Makridakis S. G., Wheelwright S. C., 1989. Forecasting methods for management, 5th ed.;
655 New York Wiley: New York, NY.
656 Mangin, A., 1984. Pour une meilleure connaissance des systemes hydrologiques à partir
657 des analyses corrélatoire et spectral [For a better knowledge of hydrological systems from
658 correlation and spectral analyzes]. J. Hydrol., 67, 25-43. https://doi.org/10.1016/0022-
659 1694(84)90230-0
660 MEA (Millennium Ecosystem Assessment), 2005. Ecosystems and Human Well-being:
661 Synthesis. Island Press, Washington, DC.
662 https://www.millenniumassessment.org/documents/document.356.aspx.pdf
663 Meeks, J., Hunkeler D., 2015. Snowmelt infiltration and storage within a karstic
664 environment, Vers Chez le Brandt, Switzerland, J. Hydrol. 529(1),11-21.
665 https://doi.org/10.1016/j.jhydrol.2015.06.040
666 Nanni, T., Rusi, S., 2003. Idrogeologia del massiccio carbonatico della montagna della
667 Majella (Appennino centrale) [Hydrogeology of the Montagna della Majella carbonate
668 massif (Central Apennines-Italy)]. Boll. Soc. Geol. It. 122, 173–202.
669 Obarti, F.J., Garay, P., Morell, I., 1988. An attempt to karst classification in Spain based on
670 system analysis. IAH 21st Congress, Karst Hydrology and Environment Karst protection,
671 10-15 October, Guilin, China.
672 Padilla, A., Pulido-Bosch, A., 1995. Study of hydrographs of karstic aquifers by means of
673 correlation and cross-spectral analysis. J. Hydrol. 168(1-4), 73–89.
674 https://doi.org/10.1016/0022-1694(94)02648-u
675 Panagopoulos, G., Lambrakis, N., 2006. The contribution of time series analysis to the
676 study of the hydrodynamic characteristics of the karst systems: Application on two typical
677 karst aquifers of Greece (Trifilia, Almyros Crete). J. Hydrol. 329, 368-376.
678 https://doi.org/10.1016/j.jhydrol.2006.02.023

679 Petalas, C., 2017. Analysis of the Hydrogeological and Hydrochemical Characteristics of
680 an Immature Karst Aquifer System. Environ. Process. 4, 603-624.
681 https://doi.org/10.1007/s40710-017-0250-y
682 Petitta, M., Mastrorillo, L., Preziosi, E., Banzato, F., Barberio, M.D., Billi, A., Cambi, C., De
683 Luca, G., Di Carlo, G., Di Curzio, D., Di Salvo, C., Nanni, T., Palpacelli, S., Rusi, S., Saroli,
684 M., Tallini, M., Tazioli, A., Valigi, D., Vivalda, P., Doglioni, C., 2018. Water-table and
685 discharge changes associated with the 2016–2017 seismic sequence in central Italy:
686 hydrogeological data and a conceptual model for fractured carbonate aquifers.
687 Hydrogeology Journal, 26, 1009-1026. https://doi.org/10.1007/s10040-017-1717-7
688 Pinault, J.L., Plagnes, V., Aquilina, L., Bakalowicz, M., 2001. Inverse modeling of the
689 hydrological and the hydrochemical behavior of hydrosystems: Characterization of karst
690 system functioning. Water Resour. Res. 37(8), 2191-2204.
691 https://doi.org/10.1029/2001WR900018
692 Polemio, M., Dragone, V., 1999. Serie storiche piezometriche delle unità idrogeologiche
693 pugliesi: regime piezometrico, effetti climatici ed antropici [Piezometric historical series of
694 Apulian hydrogeological units: piezometric regime, climatic and anthropic effects].
695 Quaderni di Geologia Applicata. 4, 153-162
696 Posavec, K., Giacopetti, M., Materazzi, M. Birk, S., 2017. Method and Excel VBA
697 Algorithm for Modeling Master Recession Curve Using Trigonometry Approach.
698 Groundwater, 55: 891-898. https://doi.org/10.1111/gwat.12549
699 Rusi, S., Di Curzio, D., Palmucci, W., Petaccia, R., 2018. Detection of the natural origin
700 hydrocarbon contamination in carbonate aquifers (Central Apennine, Italy). Environmental
701 Science and Pollution Research, 25, 15577-15596. https://doi.org/10.1007/s11356-018-
702 1769-9

703 Seidenbecher, T., Laxmi, T. R., Stork, O., Pape, H. C., 2003. Amygdalar and hippocampal
704 theta rhythm synchronization during fear memory retrieval. Science, 301(5634), 846-850.
705 https://doi.org/10.1126/science.1085818
706 Scisciani, V., Calamita, F., Bigi, S., De Girolamo, C., Paltrinieri, W. 2000. The influence of
707 syn-orogenici normal faults on Pliocene thrust system development: the Majella structure
708 (Central Apennines, Italy). Mem. Soc. Geol. It. 55, 193-204.
709 Scisciani, V., Tavarnelli, E., Calamita, F., Paltrinieri, W., 2002. Pre-thrusting normal faults
710 within syn-orogenic basins of the Outer Central Apennines, Italy: implications for Apennine
711 tectonics. Boll. Soc. Geol. It. Special Issue 1/ 2002, 295-304.
712 Thanh Tam, V., De Smedt, F., Batelaan, O., Dassargues, A., 2004. Characterization of a
713 cavern conduit system in Vietnam by time series correlation, cross-spectrum and wavelet
714 analyses. Hydrol. Sci. J., 49, 879-900. https://doi.org/10.1623/hysj.49.5.879.55140
715 Tonggang F., Hongsong C., Kelin, W., 2016. Structure and water storage capacity of a
716 small karst aquifer based on stream discharge in southwest China. Journal of Hydrology.
717 534, 50-62. https://doi.org/10.1016/j.jhydrol.2015.12.042
718 Viaroli, S., Mastrorillo, L., Lotti, F., Paolucci, V., Mazza, R., 2018. The groundwater budget:
719 A tool for preliminary estimation of the hydraulic connection between neighboring aquifers.
720 J. Hydrol. 556, 72-86. https://doi.org/10.1016/j.jhydrol.2017.10.066
721 Volatili, T., Zambrano, M., Cilona, A., Huisman, B.A.H., Rustichelli, A., Giorgioni, M.,
722 Vittori, S., Tondi, E., 2019. From fracture analysis to flow simulations in fractured
723 carbonates: The case study of the Roman Valley Quarry (Majella Mountain, Italy). Marine
724 and Petroleum Geology. 100, 95-110. https://doi.org/10.1016/j.marpetgeo.2018.10.040
725 WWAP (United Nations World Water Assessment Programme), 2015. The United Nations
726 World Water Development Report 2015: Water for a Sustainable World. Paris, UNESCO.
727 https://unesdoc.unesco.org/ark:/48223/pf0000231823